

Arene effects on difluoroboron β -diketonate mechanochromic luminescence†Tiandong Liu,^a Alan D. Chien,^a Jiwei Lu,^b Guoqing Zhang^a and Cassandra L. Fraser^{*a}

Received 11th December 2010, Accepted 2nd February 2011

DOI: 10.1039/c0jm04326e

Difluoroboron β -diketonate (BF₂bdk) dyes display reversible mechanochromic luminescence (ML) in the solid state. A series of BF₂bdk dyes with methyl, phenyl, naphthyl and anthracyl groups (*i.e.* arene substituents and bdk ligands: Me–Ph = mbm, Ph–Ph = dbm, Np–Ph = nbm, An–Ph = abm) were prepared to test the effects of π conjugation length and arene size on ML properties. Solid-state emission spectra were recorded for powders, spin-cast films, and dye coated weighing paper. The materials emit at various wavelengths from blue to red, depending on the conjugation length. Additionally, emission spectra were recorded for smeared solids and their recovery was tracked at room temperature over time. All dyes except for BF₂mbm show emission changes upon mechanical perturbation, with increasing π conjugation correlating with more dramatic, redshifted fluorescence, however, their recovery is significantly affected by the aromatic substituents. The thermal and structural properties of the dyes in the solid state were also investigated by differential scanning calorimetry (DSC) and atomic force microscopy (AFM).

Introduction

Mechanochromism is of growing research interest because molecules that change color in response to pressure can find application in dynamic functional materials, sensors, and logic gates with real-time response to mechanical stimuli. Mechanochromic luminescence (ML) refers to materials for which the emission color changes upon physical perturbation such as crushing, smearing or rubbing.¹ Though ML is a rare phenomenon, systems based on organic compounds,^{2–4} inorganic complexes,⁵ and polymers⁶ are known. Often, molecules that respond to mechanical force are organized into flexible assemblies, such as colloids, gels, or liquid crystals.^{7,8} Packing profiles reveal intermolecular interactions such as hydrogen bonding,⁸ π – π stacking,⁹ or aurophilic interactions¹⁰ but in certain cases, covalent bonds are also involved.^{11,12} Applying forces to these molecular solids can affect their packing morphology or induce a breakage or formation of new intermolecular interactions or chemical bonds. Though several mechanistic models have been advanced, structure–property relationships are still not well understood for most mechanochromic luminescent materials.

Difluoroboron β -diketonate (BF₂bdk) complexes are well-known fluorophores with intense emission both in solution and

in the solid state. Interestingly, BF₂dbks are highly sensitive to the surrounding environment. Changes in the temperature,^{13,14} solvent polarity,¹⁵ solid-state matrix,^{16,17} crystalline size,¹⁸ processing conditions and solid-state morphology^{19,20} all cause significant variation in dye emission, and recently, two new solid-state luminescent properties were discovered. For example, in poly(lactic acid) (PLA) matrices, difluoroboron dibenzoylmethane (BF₂dbm) complexes display both molecular-weight-dependent fluorescence and room temperature phosphorescence,^{21,22} useful for ratiometric oxygen sensing and tumor hypoxia imaging.^{23,24} BF₂dbm dyes also show mechanochromic luminescence in the solid-state. For instance, the emission maxima for difluoroboron avobenzene (BF₂AVB)²⁰ are 460 nm before and 542 nm after smearing. This 82 nm shift is one of the largest reported for ML molecules. A unique property of BF₂AVB is that its ML emission is reversible and rewritable after smearing. BF₂bdk dyes with alkyl chain substituents are also under investigation for their ML properties,^{25,26} and the introduction of a heavy atom allows for the production of negative images (*i.e.* scratched regions are dark, due to triplet emission quenching, or ML quenching, at room temperature).²⁷ Structure–property studies are important to gain insight into the mechanism of mechanochromic luminescence and to control emission wavelengths and recovery times. BF₂bdk dyes are ideal for this purpose because a number of analogues are known and synthetically accessible. Here, we explore the effects of simple arene substitution on ML properties by comparing BF₂ benzoylmethane systems with methyl, phenyl, naphthyl, and anthracyl substituents, namely, BF₂mbm (**1**), BF₂dbm (**2**), BF₂nbm (**3**), and BF₂abm (**4**) respectively. Both π conjugation length and steric effects are probed by this series, and different

^aDepartment of Chemistry, University of Virginia, McCormick Road, Charlottesville, VA, 22904, USA. E-mail: fraser@virginia.edu; Fax: +1 434-924-3710; Tel: +1 434-924-7998

^bDepartment of Materials Science, University of Virginia, McCormick Road, Charlottesville, VA, 22904, USA. E-mail: jl5tk@virginia.edu

† Electronic supplementary information (ESI) available: Additional emission spectra for powders, unannealed films and crystals, melting points. See DOI: 10.1039/c0jm04326e

processing conditions were tested. Samples were explored in different forms, as crystals or powders obtained from synthesis on quartz substrates, as more amorphous films spin cast from CH_2Cl_2 solutions onto glass, and as solvent cast films on weighing paper. Effects of thermal annealing and mechanical perturbation on emission and visual appearance were also studied.

Experimental

Materials

Solvents CH_2Cl_2 and THF were dried and purified by passage through alumina columns. Acetophenone, $\text{BF}_3 \cdot \text{Et}_2\text{O}$ (purified, redistilled), and all other chemicals were reagent grade from Sigma-Aldrich and were used as received without further purification.

Measurements

^1H NMR (300 MHz) spectra were recorded on a Varian Unity Inova spectrometer in CDCl_3 unless otherwise indicated. Resonances were referenced to the signal for residual protio chloroform at 7.260 ppm. ^1H NMR coupling constants are given in hertz. Mass spectra were recorded using an Applied Biosystems 4800 spectrometer with a MALDI TOF/TOF analyzer. Melting points were measured using a Laboratory Device Mel-Temp II instrument. Differential scanning calorimetry (DSC) measurements were performed using a TA Instruments DSC 2920 modulated DSC. Analyses were carried out in modulated mode under a nitrogen atmosphere (amplitude = ± 1 °C; period = 60 s; heating rate = 5 °C min^{-1} ; range -10 to 300 °C). The reported T_m and T_c values are from the first heating cycle and peak maximum values are reported. Solid state fluorescence emission spectra were recorded on a Horiba Fluorolog-3 Model FL3-22 spectrofluorometer (double-grating excitation and double-grating emission monochromators). A Laurell Technologies WS-650S spin-coater was used to cast BF_2dbks films on cover glasses for fluorescence, X-ray diffraction, and AFM measurements. Approximately 10 drops of CH_2Cl_2 solutions (1 mg mL^{-1}) were spun for 1 min at a rotator speed of 2000 rpm. Films on weighing paper were prepared by applying several drops of CH_2Cl_2 sample solution (1 mg mL^{-1}) onto the paper substrate and allowing the surface to dry under air. The weighing paper was then taped to the outside of a glass vial for ease of smearing and luminescence analysis. The photograph in Fig. 3 was taken with an Apple iPhone 4 digital camera with the default setting (no flash). Tapping mode AFM (DI 3000, Digital Instrument, CA) was used to characterize the morphology of spin cast films with a scan rate of 0.8 Hz over an area of 20×20 μm .

Synthesis of β -diketones

The methyl (mbm), naphthyl (nbm) and anthracyl (abm) β -diketone ligands were prepared by Claisen condensation in the presence of NaH as previously described.²⁸ (Note: mbm and dbm are commercially available from Aldrich.)

2-Naphthoyl benzoyl methane (nbm). Acetophenone (500 mg, 4.12 mmol), methyl-2-naphthoate (1.03 g, 5.36 mmol) and THF

(20 mL) were added sequentially to a 50 mL round bottom flask. After stirring the mixture for 10 min, a suspension containing NaH (167 mg, 6.61 mmol) in THF (10 mL) was added dropwise at room temperature under N_2 . The mixture was stirred for 20 h before saturated aqueous NaHCO_3 (1 mL) was added to quench the reaction. THF was removed *in vacuo* before 1 M HCl (20 mL) was added. The aqueous phase was extracted with CH_2Cl_2 (3×20 mL). The combined organic layers were washed with distilled water (2×10 mL) and brine (10 mL), and dried over Na_2SO_4 before concentration *in vacuo*. The residue was purified by column chromatography on silica gel eluting with hexanes/ethyl acetate (6 : 1) to give 2-naphthoyl benzoylmethane, nbm, as a yellow solid: 700 mg (62%). ^1H NMR (300 MHz, CDCl_3) δ 16.98 (s, 1H, ArCOH), 8.62 (s, 1H, 1'-ArH), 8.08–7.87 (m, 6H, 3',4',5',8'-ArH, 2'',6''-ArH), 7.62–7.49 (m, 5H, 6',7'-ArH, 3'',4'',5''-ArH), 7.01 (s, 1H, COCHCO); MS (MALDI) m/z = 275.13 ($M + \text{H}^+$), calcd m/z = 275.11.

2-Anthracenoyl benzoyl methane (abm). The anthracyl ligand was prepared from 2-acetyl anthracene (301 mg, 1.34 mmol) and methyl benzoate (252 μL , 2.01 mmol) as described for nbm except that 3 equivalents of NaH were used and the reaction was refluxed for 12 h. After purification by column chromatography (3 : 1 hexanes/EtOAc to remove impurities, then CH_2Cl_2 to elute the product), the diketone, abm, was obtained as a red solid: 362 mg (84%). ^1H NMR (300 MHz, CDCl_3) δ 16.96 (s, 1H, ArCOH), 8.75 (s, 1H, 1'-ArH), 8.60 (s, 1H, 10'-ArH), 8.46 (s, 1H, 9'-ArH), 8.10–7.95 (m, 6H, 3',4',5',8'-ArH, 2'',6''-ArH), 7.61–7.50 (m, 5H, 6',7'-ArH, 3'',4'',5''-ArH), 7.01 (s, 1H, COCHCO); MS (MALDI) m/z = 324.07 ($M + \text{H}^+$), calcd m/z = 324.12.

Difluoroboron-diketonate synthesis

A representative synthesis is provided for difluoroboron 2-naphthoyl benzoyl methane (BF_2nbm) (3).

Difluoroboron 2-naphthoyl benzoyl methane, BF_2nbm (3). Boron trifluoride diethyl etherate (88 μL , 0.70 mmol) was added to a solution of 2-naphthoyl benzoyl methane (191 mg, 0.70 mmol) in CH_2Cl_2 (20 mL) under N_2 . After stirring the mixture at room temperature for 12 h, the solvent was removed *in vacuo*. (Note: under reflux, boronation reactions are complete after ~ 1 to 2 h.) The residue was recrystallized from acetone to give BF_2nbm as a yellow powdery solid: 147 mg (65%). Data are in accord with literature values.¹⁰ ^1H NMR (300 MHz, CDCl_3) δ 8.80 (s, 1H, 1'-ArH), 8.22 (d, $J = 8.1$, 2H, 2'',6''-ArH), 8.10–7.92 (m, 4H, 3',4',5',8'-ArH), 7.73–7.59 (m, 5H, 6',7',3'',4'',5''-ArH), 7.35 (s, 1H, COCHCO); MS (MALDI) m/z = 345.00 ($M + \text{Na}^+$), calcd m/z = 345.09.

Difluoroboron acetyl benzoyl methane, BF_2mbm (1). Pale yellow needle-like crystals precipitated from acetone/hexanes.²⁹ ^1H NMR (300 MHz, CDCl_3) δ 8.08–8.04 (m, 2H, 2',6'-ArH), 7.72–7.66 (m, 1H, 4'-ArH), 7.56–7.50 (m, 2H, 3',5'-ArH), 6.59 (s, 1H, COCHCO), 2.42 (s, 3H, CH_3CO); MS (MALDI) m/z = 233.02 ($M + \text{Na}^+$), calcd m/z = 233.06.

Difluoroboron dibenzoyl methane, BF_2dbm (2). Pale yellow powder precipitated from acetone/hexanes. Data are in accord

with literature values.¹⁵ ¹H NMR (300 MHz, CDCl₃) δ 8.19–8.15 (m, 4H, 2',6'-ArH, 2'',6''-ArH), 7.74–7.68 (m, 2H, 4'-ArH, 4''-ArH), 7.60–7.54 (m, 4H, 3',5'-ArH, 3'',5''-ArH), 7.21 (s, 1H, COCHCO); MS (MALDI) *m/z* = 295.06 (M + Na⁺), calcd *m/z* = 295.07.

Difluoroboron 2-anthracenyl benzoyl methane, BF₂abm (4).

Boron trifluoride diethyl etherate (210 μL, 1.67 mmol) was added dropwise to a stirred solution of 2-anthracenyl benzoyl methane (abm) (362 mg, 1.12 mmol) in CH₂Cl₂ (20 mL) under N₂. After stirring the mixture at room temperature for 12 h, saturated aqueous NaHCO₃ (1 mL) was added to quench the reaction. (Note: under reflux, boronation reactions are complete after ~1 to 2 h.) The aqueous phase was extracted with CH₂Cl₂ (3 × 20 mL) and the combined organic layers were washed with distilled water (2 × 10 mL) and brine (10 mL), and dried over Na₂SO₄ before concentration *in vacuo*. The residue was recrystallized from acetone to give BF₂abm as a red powdery solid: 186 mg (42%). ¹H NMR (300 MHz, CDCl₃) δ 9.02 (s, 1H, 1'-ArH), 8.65 (s, 1H, 9'-ArH), 8.47 (s, 1H, 10'-ArH), 8.23–7.97 (m, 6H, 3',4',5',8'-ArH, 2'',6''-ArH), 7.74–7.52 (m, 5H, 6',7',3'',4'',5''-ArH), 7.36 (s, 1H, COCHCO); MS (MALDI) *m/z* = 395.05 (M + Na⁺), calcd *m/z* = 395.10.

Results and discussion

Dye synthesis

Boron dyes **1–4** were synthesized *via* a previously reported method.²³ Namely, the diketone ligand precursors were obtained by Claisen condensation between appropriate ketones and esters, using NaH as the base to deprotonate the ketones in all cases. The anthracene ligand, abm, requires three equivalents NaH and refluxing conditions for 12 hours, whereas the other ligands can be produced at room temperature after 12 hours or less with lower base loadings (*i.e.* 1.5 equivalents *vs.* the ketone). Ligands show good solubility in common organic solvents such as CH₂Cl₂ and EtOAc, with the exception of abm which shows poor solubility in EtOAc. The reaction between boron trifluoride etherate (BF₃·Et₂O) and the corresponding β-diketones in refluxing dichloromethane generates the difluoroboron-diketone products **1–4** within two hours, in moderate yield after recrystallization (*e.g.* **3**: 65% yield). Sample **1** was obtained as needle-shaped crystals and **2–4** as powders.

Solid-state emission color

For an initial comparison of fluorescence colors, dyes were investigated as powders, spin-cast films on glass, and solvent cast films on weighing paper. As isolated, solid-state boron dyes **1–4** (λ_{em} , nm) show cyan (433; crystals), green-yellow (531, with high energy peak at 446; microcrystalline powder), green (512; powder), and red (643; powder) emission respectively (λ_{ex} = 365 nm) (Table 1, Fig. S1, ESI†). Amorphous films of dyes **1–4** were generated by spin casting methylene chloride solutions (10 drops, 1 mg mL⁻¹) onto glass (1 × 1 in). After air drying for at least two hours, spectra were recorded under ambient atmosphere (Table 2, Fig. 1). More sample (20 drops, 1 mg mL⁻¹) was used to generate films for the images to better visualize the colors and their changes upon thermal annealing. Fig. 1 illustrates that

Table 1 Emission maxima and bandwidths for powders **1–4** on quartz^a

BF ₂ bd	λ_{P}	λ_{TA}	λ_{S}	fwhm _P	fwhm _{TA}	fwhm _S
BF ₂ mbm (1)	433	429	434	87	87	90
BF ₂ dbm (2)	531	529	534	100	110	101
BF ₂ nbm (3)	512	511	515	63	63	95
BF ₂ abm (4)	643	622	634	117	115	117

^a P = powder; TA = thermally annealed; S = smeared; fwhm = full width at half maximum. Units are shown in nm.

the fluorescence colors for the films range from blue to red in this series (**1**: blue; **2**: yellow-green; **3**: green; **4**: red), further demonstrating that solid-state emission color is readily modulated by arene substitution. Emission from the anthracene derivative **4** is very dim compared to the other analogues; hence, the films look dark in Fig. 1. Emission maxima, λ_{em} , span a ~200 nm range for this film sample set: BF₂mbm: 434 nm, BF₂dbm: 534 nm, BF₂nbm: 502 nm, and BF₂abm: 641 nm. Emission colors on weighing paper are comparable to spin-cast films on glass, and qualitative tests with filter paper as a substrate, commonly used for vapochromism studies,³⁰ are also similar.

Generally, emission maxima show a bathochromic shift with extended π conjugation of the aromatic moieties; however, the phenyl-naphthyl derivative **3** emits at a shorter wavelength than the diphenyl dye **2**, which is an exception to this trend. There is growing evidence in solution and computational studies to suggest that the entire ligand structure influences emission for symmetrical structures like dbm; whereas, in unsymmetrical structures, it is the larger arene donor that dominates in intramolecular charge transfer (ICT) processes.²⁴ These results suggest that this may extend to solid state emission as well; however here, differential intermolecular interactions and dye-dye stacking between dbm and nbm systems could also be playing an important role. In this case, BF₂dbm may have stronger intermolecular interactions (ground- and excited-state dimers) than BF₂nbm.

Thermal annealing

The melting point and melting and crystallization temperatures (°C) of the dyes were measured by DSC (Table 3). Temperatures increase with molecular weight as expected. No additional phase transitions were noted.

Spin-cast films of **1–4** were annealed at 110 °C for 10 minutes and associated normalized emission spectra are provided in Fig. 1B. The spectrum for the methyl derivative BF₂mbm, **1**,

Table 2 Emission maxima and bandwidths for spin-cast films **1–4** on glass^a

BF ₂ bdk	λ_{A}	λ_{TA}	λ_{S}	fwhm _A	fwhm _{TA}	fwhm _S
BF ₂ mbm (1)	434	435	433	83	79	82
BF ₂ dbm (2)	534	531	541	100	109	102
BF ₂ nbm (3)	502	487	516	96	76	109
BF ₂ abm (4)	641	584	636	123	162	117

^a A = amorphous; TA = thermally annealed, S = smeared; fwhm = full width at half maximum. Units are shown in nm

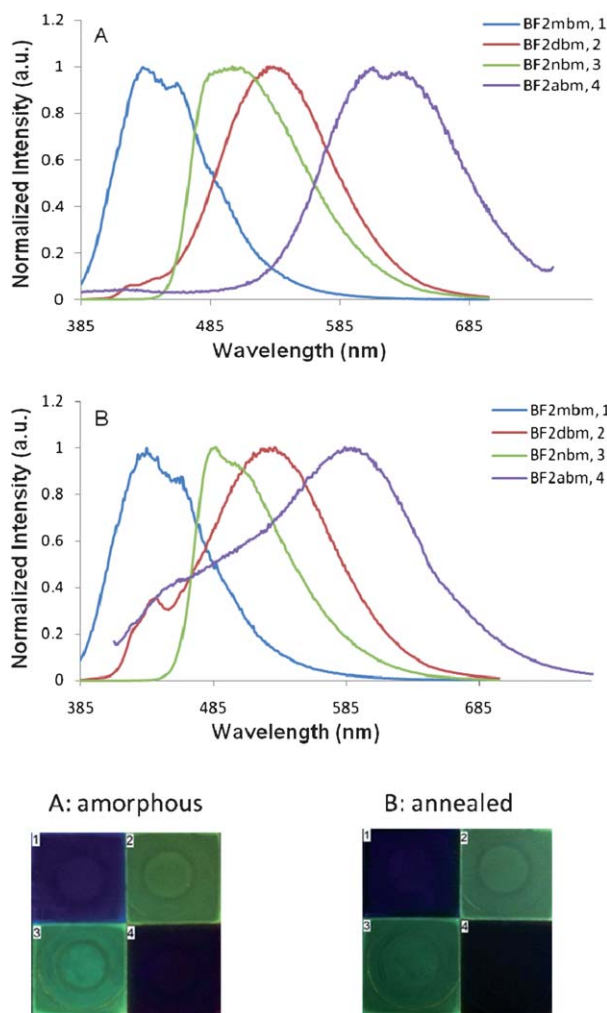


Fig. 1 Solid-state emission spectra and images of **1–4** as films spin-cast from CH_2Cl_2 solutions (1 mg mL^{-1}) onto glass. (A) Before (amorphous) and (B) after thermal annealing. (**1–3**: $\lambda_{\text{ex}} = 369 \text{ nm}$; **4**: $\lambda_{\text{ex}} = 397 \text{ nm}$.)

Table 3 Melting and crystallization temperatures for boron dyes **1–4**

BF ₂ bdk	T_m^a	T_c^a
BF ₂ mbm (1)	157	130
BF ₂ dbm (2)	193	181
BF ₂ nbm (3)	228	210
BF ₂ abm (4)	254	214

^a DSC; peak values.

showed little change upon annealing, but the intensity decreased. The emission spectrum of BF₂dbm, **2**, slightly blue shifted (~ 2 to 3 nm), broadened (fwhm increased ~ 9 to 10 nm), and a new peak emerged at $\sim 440 \text{ nm}$ (Tables 1 and 2). In previous studies, the short wavelength band has been attributed to monomeric emission, which authors say is more prominent in larger crystals.⁸ (Compare to BF₂dbm $\lambda_{\text{em}} = 417 \text{ nm}$ in CH_2Cl_2 .) However, aggregate emission states may be a more likely explanation. The aggregation behavior of dyes has been extensively studied and has been classified into H-aggregates and J-aggregates based on the slippage angle, which is defined as the angle between the line

connecting the centers of the adjacent dye molecules and the long axis of a molecule.³¹ If the angle is small (*e.g.*, less than 32° for cyanine dyes), aggregation will induce a bathochromic shift in absorption and emission, which is called J-aggregates. Aggregation causes a hypsochromic shift when the angle is larger than 32° for cyanine dyes and is attributed to H-aggregates. The previously reported crystallography data of BF₂dbm⁸ revealed a slippage angle of $\sim 25^\circ$. If this small angle is associated with J-aggregates for this system too, it could maybe explain the emergence of the small peak at 440 nm that arises upon thermally annealing and is bathochromically shifted relative to monomer emission. The hypsochromic shift of the main emission peak for BF₂dbm after heating may also be ascribed to aggregation in the crystalline structures that form. A dramatic blue shift was observed previously for crystalline BF₂AVB²⁰ and BF₂dbmOC₁₂H₂₅ states.²⁵

Previously, it was reported that BF₂dbm tends to form different stacking profiles. Two types of arrangements are common.^{8,32} In the first case, the phenyl rings of adjacent BF₂dbm molecules overlap. In the second case, the diketonate and a phenyl ring of two adjacent molecules stack. In both cases, adjacent boron diketonates moieties face in opposite directions. When the dye solids were heated, the distance between the overlapping molecules increased,⁸ which implies that the observed spectral changes may be associated with a change in interdimeric interactions. Reasons for these arrangements are not known, but the strong electron withdrawing difluoroboron group may function as a directing unit and arranging large dipoles opposite to each other may increase the distance, and lower the repulsion and overall energy of the system. Compared to BF₂dbm, the emission spectrum of BF₂nbm is more narrow; the lower energy side of the peak is absent. An amorphous spin-cast BF₂nbm has a major peak at 502 nm accompanied by a shoulder at 487 nm , which may arise from the amorphous and ordered aggregate emission respectively. The monomeric emission of BF₂nbm in methylene chloride solution is at 483 nm , which could also be a contributing factor in the solid state. Here too, the relative intensity of the blueshifted peak was enhanced after thermal annealing and the full width at half maximum (fwhm) narrowed from 96 nm to 76 nm for the spin-cast film, similar to previous observations with BF₂AVB.²⁰

In contrast to the nbm complex, BF₂abm exhibited a dramatic hypsochromic shift after annealing, so differences do not arise from size alone. For example, for the amorphous film of **4**, the emission maxima shifted from 641 nm to 584 nm (57 nm), the peak broadened considerably, with an increased intensity blue shoulder for BF₂abm. Here too, the dramatic hypsochromic shift may originate from aggregation. (Compare to BF₂abm in dilute solution: $\lambda_{\text{em}} = 595 \text{ nm}$.)

To gain further insight into the solid-state morphology and ways that samples change upon heating, atomic force microscopy (AFM) was employed (Fig. 2). As-spun films had similar ring-like morphologies upon evaporation of solvent by spin-casting. Data confirm the aggregation of compounds **1–3** after thermal treatment. BF₂mbm may sublime or decompose during thermally annealing, consistent with decreased emission intensity in the image in Fig. 1B, however, it still formed larger bead-shaped species. For BF₂dbm and BF₂nbm, square- and triangle-shaped crystalline species were observed respectively. BF₂abm

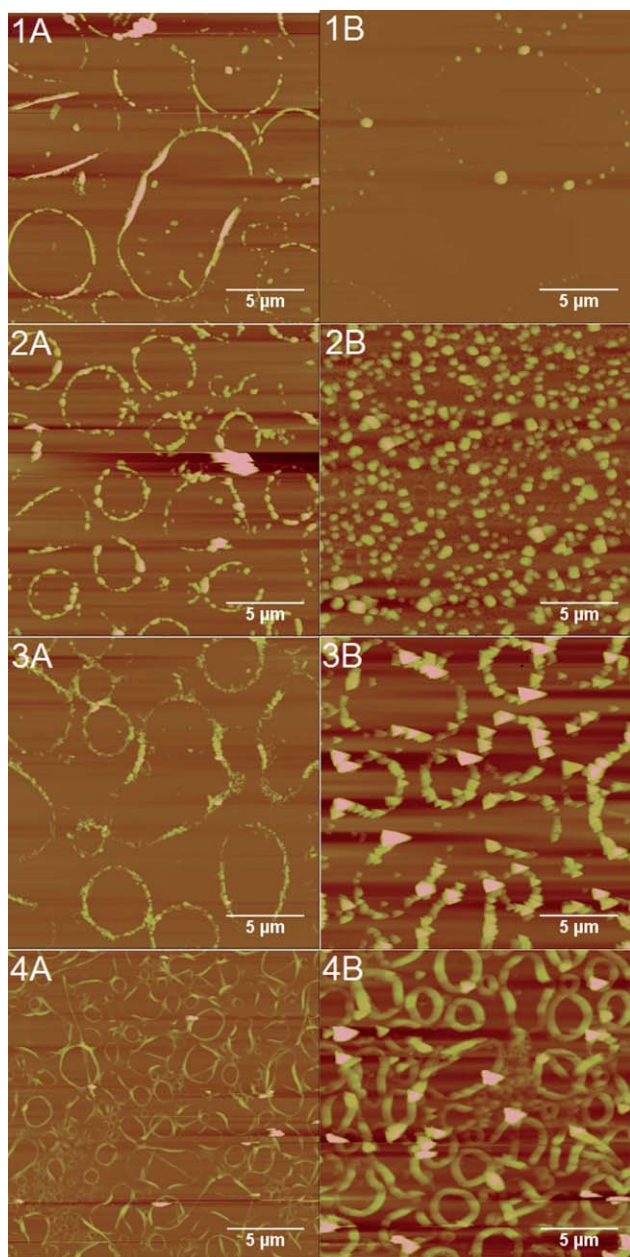


Fig. 2 AFM images of BF₂mbm (1), BF₂dbm (2), BF₂nbm (3), and BF₂abm (4) spin-cast films on glass substrates. A = as-spun films and B = after thermal annealing.

samples formed larger rings after annealing, but it is not as obvious visually that crystalline species emerged. Generally speaking, compounds 2–4 show increased crystallinity, greater or lesser hypsochromic shifts and a new emission peak at short wavelength after thermally annealing. H aggregates may be involved.

Mechanochromic luminescence

Mechanical responsiveness of the dyes was also tested for crystalline and powdery solids obtained from synthesis as well as for thermally annealed spin-cast films. BF₂mbm and BF₂dbm crystalline solids showed significant changes in emission when they

were smeared (Fig. S2, ESI[†]). For example, the crystalline BF₂dbm has two emission peaks at 446 nm and 522 nm respectively. However, only a broader longer wavelength emission still existed when the crystals were crushed. Mirochnik attributed this to size-dependent fluorescence in solid state BF₂dbks. The short wavelength peak was assigned to the monomeric emission, which only appeared in large-sized crystals and the long wavelength peak was assigned to interdimeric associations.¹² An alternative explanation is that the original sample has both ordered and amorphous components. When the sample is crushed, the short wavelength peak associated with crystalline aggregate emission disappears and a more disordered, amorphous state is generated, which gives rise to a broad, redshifted emission.

In attempts to distinguish mechanochromism from size dependent crystalline emission, 1–4 powders were applied to the surface of a quartz cuvette and the emission properties were investigated after smearing (Fig. 3). Thermally annealed spin-cast films were also monitored after smearing for comparison (Fig. 4). These experiments show that aromatic groups influence BF₂bdk ML properties—the presence or absence of mechanoresponsiveness, the emission wavelength shift, and the recovery rate—in measurable ways. Processing methods can play a role too. Mechanochromic effects of each dye, 1–4, will be discussed in turn below.

The emission spectrum of solid BF₂mbm, 1, has a major peak at 433 nm accompanied by a shoulder peak at 459 nm (Fig. 3A), the shoulder emission of the powder species only slightly increasing after thermally annealing at 110 °C for 10 min. Mechanical perturbation removed the enhancement of the shoulder peak, and resulted in an emission spectrum that matches the less ordered sample before annealing. Amorphous films of BF₂mbm are even less responsive to mechanical force (Fig. 4A). Emission spectra are nearly identical for spin-cast, annealed and smeared films. Correspondingly, for films too, no visible color change is noted. Thus, under the conditions tested, BF₂mbm cannot be considered mechanochromic.

The ML behaviors of BF₂dbm are shown in Fig. 3B and 4B. The emission spectra of smeared BF₂dbm powders and films were nearly identical to respective amorphous powder and film samples before annealing. The short wavelength emission that emerged after annealing disappeared, which may be interpreted as the loss of the aggregated species. In tracking the emission of the smeared samples over time, they kept blueshifting gradually until the main emission overlapped with that of the ordered, thermally annealed sample. Notably, recovery dynamics of BF₂dbm powders and films have significant differences. The films on glass recovered in less than 2 hours, whereas the powders on the quartz cuvette took up to a day to return to the initial thermally annealed state. Clearly, BF₂dbm aggregated and formed a thermally preferred structure, which induced the hypsochromic shift. Mechanical force disrupted the organization in the thermally stable structure. This process is represented by the red-shift in emission after the smearing.

For BF₂nbm, mechanochromic luminescent effects are manifested differently. The emission maximum ($\lambda_{em} = 513$ nm) of the powder on a quartz substrate did not change before and after annealing (Fig. 3C); however, the emission peak was drastically broadened after smearing. The fwhm increased from 62 nm to 96 nm. In the first ten minutes after smearing, the bandwidth

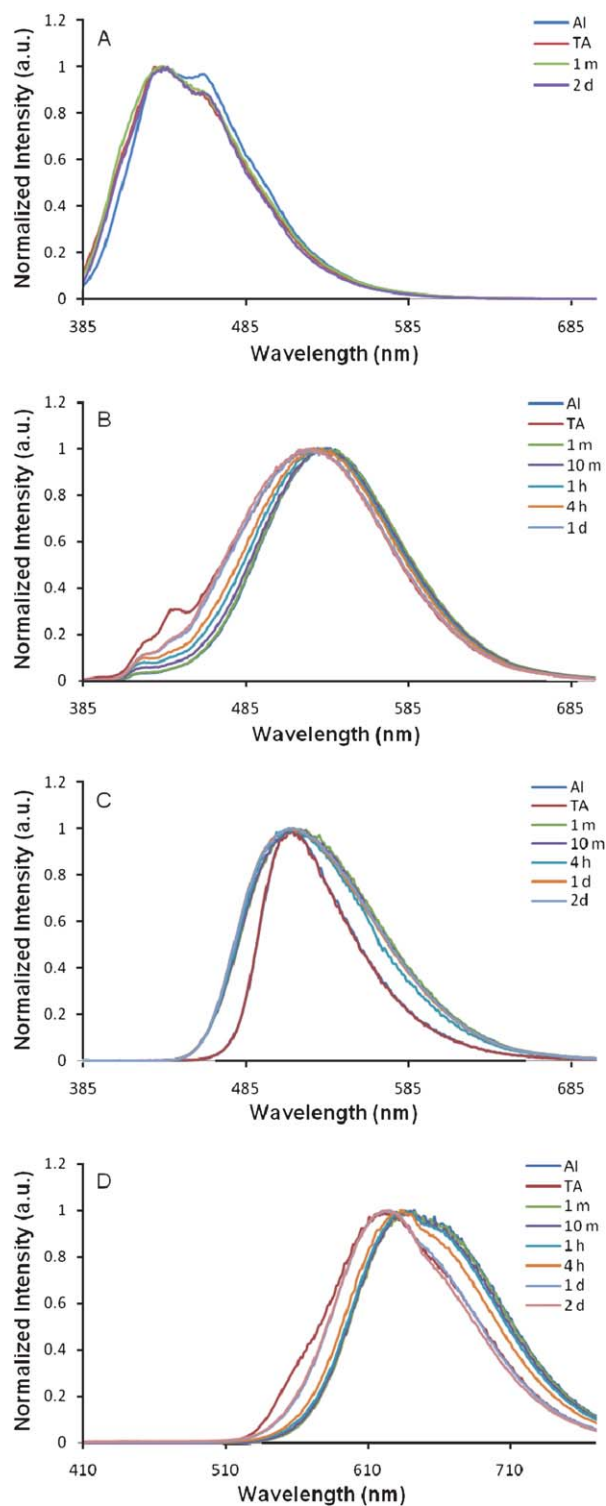


Fig. 3 Normalized emission spectra of 1–4 powders on quartz. (A) BF₂mbm, $\lambda_{\text{ex}} = 369$ nm. (B) BF₂dbm, $\lambda_{\text{ex}} = 369$ nm. (C) BF₂nbm, $\lambda_{\text{ex}} = 369$ nm. (D) BF₂abm, $\lambda_{\text{ex}} = 397$ nm. (AI = as isolated powder; TA = thermally annealed powder; times indicate after smearing; m = minute, h = hour, d = day).

narrowed slightly, but after that, the spectra remained unchanged after monitoring for two days. Of the difluoroboron dyes that we have investigated in this way, BF₂nbm is the first

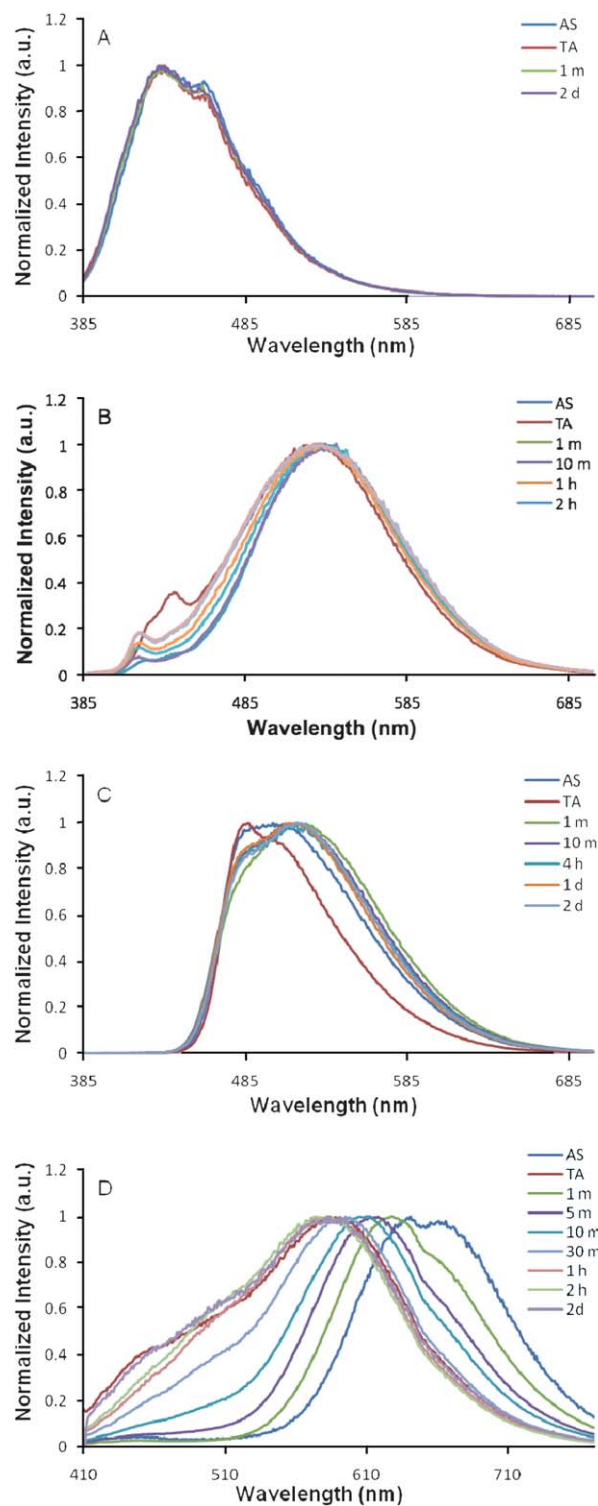


Fig. 4 Normalized emission spectra of amorphous films of 1–4 on cover glass. (A) BF₂mbm, $\lambda_{\text{ex}} = 369$ nm. (B) BF₂dbm, $\lambda_{\text{ex}} = 369$ nm. (C) BF₂nbm, $\lambda_{\text{ex}} = 369$ nm. (D) BF₂abm, $\lambda_{\text{ex}} = 397$ nm. (AS = as-spun film; TA = thermally annealed film; times indicate after smearing; m = minute, h = hour, d = day).

one that is largely stable after smearing. Clearly, the aromatic substituent is not just influencing the emission maxima, but the recovery dynamics too.

Table 4 Lifetimes of spin-cast films of **1–4** on cover glass

BF ₂ dbk	τ_A^a	τ_{TA}^a	τ_S^a
BF ₂ mbm (1)	8.9	—	—
BF ₂ dbm (2)	51.5	48.6	51.3
BF ₂ nbm (3)	15.0	11.9	15.5
BF ₂ abm (4)	5.0	7.3	3.0

^a A = amorphous, TA = thermally annealed, S = smeared. Units are shown in ns

The dye with the even larger anthracene ring, BF₂abm, showed the most dramatic emission change upon smearing. The emission maximum shift from 622 nm to 634 nm for the powder sample (Fig. 3D) and from 584 nm to 636 nm for the thermally annealed spin-cast film (Fig. 4D). Whether starting from the powder or the film, smeared samples revert to the starting thermally annealed emission, but the recovery rates are distinctly different. It takes up to a day for the powder sample to recover, but only an hour for the smeared spin-cast BF₂abm film to return to the initial. In both cases, the shoulder emission does not reappear, also suggesting that it arises from thermally induced aggregation.

Thermal annealing is a key factor in observing ML for this arene series. When mechanical perturbation was applied to unannealed spin-cast **1–4** films on cover glass, their emission spectra showed much less change compared to the annealed samples (Fig. S3, ESI†). As has been observed previously for BF₂dbmOC₁₂H₂₅, spin-cast films and mechanically smeared samples show spectral similarity, suggesting that both are amorphous states. Multiple interactions, such as strong dipolar nature of the molecules, arene stacking and Ar–H···F hydrogen bonds, may be the driving force for the aggregation of BF₂mbm, BF₂dbm, and BF₂nbm, upon thermal treatment or recovery after smearing.

The lifetimes of the spin-cast samples were also monitored (Table 4). For BF₂dbm and BF₂nbm, the lifetimes slightly decreased after annealing. But the smeared samples have nearly identical lifetimes as the original samples, as could be expected, given both are more amorphous states. BF₂abm undergoes a different process. Compared to the initial amorphous spin-cast state, the lifetime increased after annealing but then decreased significantly after smearing. Taken together, the AFM and emission data point to different behavior for BF₂abm after thermal treatment and smearing. The reasons for this are not clear.

Conclusion

The aromatic substituents in boron diketonates **1–4** significantly influence the solid-state emission properties, both emission maxima and mechanochromic luminescence too. BF₂mbm, **1**, is not mechanochromic under the conditions tested, whereas **2–4** exhibit unique ML properties, and increasingly more pronounced differences between as-spun and annealed states. These trends may be due, in part, to differences in the T_m values for these systems. For the lower molecular weight dyes, glass transition temperatures ($\sim 2/3 T_m$) more nearly approach room temperature, and dyes may begin to slowly crystallize even under ambient conditions. As-spun and mechanically perturbed

samples may not be fully amorphous at room temperature. This was verified by XRD, that indicated some degree of crystallinity for as-spun films of **1**, but not for **2–4**. Generally, emission maxima redshift with increasing arene conjugation and after smearing, the shift to lower energy becomes more distinct. The dye containing the naphthyl unit showed unrecoverable emission after mechanical perturbation, whereas the emissions of smeared BF₂dbm and BF₂abm move towards short wavelength and resemble the initial thermally annealed state over time. The amorphous film species recover faster than the powders, which may be a sample thickness effect. For these samples, thermal annealing is the key step to observing mechanochromic luminescence, in a pronounced way or at all. When unannealed samples are smeared, little change is observed in the spectra. AFM studies revealed that **2–4** aggregated during annealing and formed crystalline species, which are associated with the emergence or increase of a higher energy emission band, perhaps due to aggregate emission. The lifetimes of the smeared samples and original amorphous film samples are in accord, which implies that smearing also generates an amorphous state. Overall, the formation and disappearance of the aggregated species appears to be the reason for the luminescence variation upon thermally annealing and mechanical perturbation, and strong intermolecular interactions may be the driving force for thermally induced aggregation and spontaneous recovery at room temperature after smearing.²⁰

In this study, solid-state dyes with different arene substituents were explored. Numerous questions remain regarding steric and electronic effects on mechanochromic luminescence properties. Furthermore, substrate effects and quantifying the sensitivity of the dyes to force also merit investigation. These topics, ways of modulating the luminescence response, and uses for mechanochromic luminescent materials will serve as the subjects of future reports.

Acknowledgements

We thank the National Science Foundation for support for this research (CHE 0718879) and we thank the Beckman Foundation for a Beckman Scholarship to Alan D. Chien and generous support of undergraduate research at UVA.

References

- 1 Y. Sagara and T. Kato, *Nat. Chem.*, 2009, **1**, 605–610.
- 2 X. Zhang, Z. Chi, H. Li, B. Xu, X. Li, W. Zhou, S. Liu, Y. Zhang and J. Xu, *Chem.-Asian J.*, 2011, DOI: 10.1002/asia.201000802.
- 3 Y. Ooyama, Y. Kagawa, H. Fukuoka, G. Ito and Y. Harima, *Eur. J. Org. Chem.*, 2009, 5321–5326; Y. Ooyama, G. Ito, H. Fukuoka, T. Nagano, Y. Kagawa, I. Imae, K. Komaguchi and Y. Harima, *Tetrahedron*, 2010, **66**, 7268–7271.
- 4 J. Kunzelman, M. Kinami, B. R. Crenshaw, J. D. Protasiewicz and C. Weder, *Adv. Mater.*, 2008, **20**, 119–122.
- 5 Y.-A. Lee and R. Eisenberg, *J. Am. Chem. Soc.*, 2003, **125**, 7778–7779.
- 6 C. Löwe and C. Weder, *Adv. Mater.*, 2002, **14**, 1625–1629; B. R. Crenshaw and C. Weder, *Chem. Mater.*, 2003, **15**, 4717–4724; M. Kinami, B. R. Crenshaw and C. Weder, *Chem. Mater.*, 2006, **18**, 946–955.
- 7 Y. Sagara, S. Yamane, T. Mutai, K. Araki and T. Kato, *Adv. Funct. Mater.*, 2009, **19**, 1869–1875; V. N. Kozhevnikov, B. Donnio and D. W. Bruce, *Angew. Chem., Int. Ed.*, 2008, **47**, 6286–6289.
- 8 Y. Sagara and T. Kato, *Angew. Chem., Int. Ed.*, 2008, **47**, 5175–5178.

- 9 J. W. Chung, Y. You, H. S. Huh, B.-K. An, S.-J. Yoon, S. H. Kim, S. W. Lee and S. Y. Park, *J. Am. Chem. Soc.*, 2009, **131**, 8163–8168; S.-J. Yoon, J. W. Chung, J. Gierschner, K. S. Kim, M.-G. Choi, D. Kim and S. Y. Park, *J. Am. Chem. Soc.*, 2010, **132**, 13675–13683; Y. Sagara, T. Mutai, I. Yoshikawa and K. Araki, *J. Am. Chem. Soc.*, 2007, **129**, 1520–1521.
- 10 H. Ito, T. Saito, N. Oshima, N. Kitamura, S. Ishizaka, Y. Hinatsu, M. Wakeshima, M. Kato, K. Tsuge and M. Sawamura, *J. Am. Chem. Soc.*, 2008, **130**, 10044–10045.
- 11 D. A. Davis, A. Hamilton, J. Yang, L. D. Cremer, D. V. Gough, S. L. Potisek, M. T. Ong, P. V. Braun, T. J. Martinez, S. R. White, J. S. Moore and N. R. Sottos, *Nature*, 2009, **459**, 68–72; G. O'Bryan, B. M. Wong and J. R. McElhanon, *ACS Appl. Mater. Interfaces*, 2010, **2**, 1594–1600.
- 12 R. A. Koevoets, S. Karthikeyan, P. C. M. M. Magusin, E. W. Meijer and R. P. Sijbesma, *Macromolecules*, 2009, **42**, 2609–2617.
- 13 A. G. Mirochnik, E. V. Fedorenko, B. V. Bukvetskii and V. E. Karasev, *Russ. Chem. Bull.*, 2005, **54**, 1060–1062.
- 14 A. G. Mirochnik, E. V. Fedorenko, B. V. Bukvetskii, V. G. Kuryavii and V. E. Karasev, *J. Fluoresc.*, 2006, **16**, 279–286.
- 15 E. Cogné-Laage, J.-F. Allemand, O. Ruel, J.-B. Baudin, V. Croquette, M. Blanchard-Desce and L. Jullien, *Chem.–Eur. J.*, 2004, **10**, 1445–1455.
- 16 G. Zhang, T. L. St. Clair and C. L. Fraser, *Macromolecules*, 2009, **42**, 3092–3097; G. Zhang, G. L. Fiore, T. L. St. Clair and C. L. Fraser, *Macromolecules*, 2009, **42**, 3162–3169.
- 17 A. G. Mirochnik, E. V. Gukhman, P. A. Zhikhareva and V. E. Karasev, *Spectrosc. Lett.*, 2002, **35**, 309–315.
- 18 A. G. Mirochnik, E. V. Fedorenko, A. A. Karpenko, D. A. Gizzatulina and V. E. Karasev, *Luminescence*, 2007, **22**, 195–198; A. G. Mirochnik, E. V. Fedorenko and V. E. Karasev, *Russ. Chem. Bull.*, 2008, **57**, 1190–1193.
- 19 G. F. Manbeck, W. W. Brennessel, R. A. Stockland, Jr. and R. Eisenberg, *J. Am. Chem. Soc.*, 2010, **132**, 12307–12318.
- 20 G. Zhang, J. Lu, M. Sabat and C. L. Fraser, *J. Am. Chem. Soc.*, 2010, **132**, 2160–2162.
- 21 G. Zhang, J. Chen, S. J. Payne, S. E. Kooi, J. N. Demas and C. L. Fraser, *J. Am. Chem. Soc.*, 2007, **129**, 8942–8943.
- 22 G. Zhang, R. E. Evans, K. A. Campbell and C. L. Fraser, *Macromolecules*, 2009, **42**, 8627–8633.
- 23 G. Zhang, G. M. Palmer, M. W. Dewhirst and C. L. Fraser, *Nat. Mater.*, 2009, **8**, 747–751.
- 24 G. M. Palmer, A. N. Fontanella, G. Zhang, G. Hanna, C. L. Fraser and M. W. Dewhirst, *J. Biomed. Opt.*, 2010, **15**, 066021.
- 25 G. Zhang, J. P. Singer, R. E. Evans, S. E. Kooi, E. L. Thomas and C. L. Fraser, *J. Mater. Chem.*, DOI: 10.1039/c0jm03871g.
- 26 N. D. Nguyen, A. E. Sherman, J. Lu, G. Zhang and C. L. Fraser, *J. Mater. Chem.*, 2011, DOI: 10.1039/c1jm00067e.
- 27 G. Zhang, J. Lu and C. L. Fraser, *Inorg. Chem.*, 2010, **49**, 10747–10749.
- 28 J. L. Bender, P. S. Corbin, C. L. Fraser, D. H. Metcalf, F. S. Richardson, E. L. Thomas and A. M. Urbas, *J. Am. Chem. Soc.*, 2002, **124**, 8526–8527.
- 29 G. Zhang, S. Xu, T. Liu, R. E. Evans, N. Nguyen and C. L. Fraser, in preparation.
- 30 T. J. Waldas, Q.-M. Wang, Y.-J. Kim, C. Flaschenreim, T. N. Blanton and R. Eisenberg, *J. Am. Chem. Soc.*, 2004, **126**, 16841–16849.
- 31 M. Shimizu and T. Hiyama, *Chem.–Asian J.*, 2010, **5**, 1516–1531.
- 32 A. G. Mirochnik, B. V. Bukvetskii, E. V. Gukhman, P. A. Zhikhareva and V. E. Karasev, *Izv. Akad. Nauk, Ser. Khim.*, 2001, **50**, 1535 [*Russ. Chem. Bull., Int. Ed.*, 2001, 1612].